

---

# SPECTRAL EMBEDDING VIA CHEBYSHEV BASES FOR ROBUST DEEPONET APPROXIMATION

---

A PREPRINT

**Muhammad Abid**

Department of Mechanical and Aerospace Engineering,  
University of Tennessee,  
Knoxville, TN 37996, USA.  
mabid@vols.utk.edu

**Omer San**

Department of Mechanical and Aerospace Engineering,  
University of Tennessee,  
Knoxville, TN 37996, USA.  
osan@utk.edu

## ABSTRACT

Deep Operator Networks (DeepONets) have become a central tool in data-driven operator learning, providing flexible surrogates for nonlinear mappings arising in partial differential equations (PDEs). However, the standard trunk design based on fully connected layers acting on raw spatial or spatiotemporal coordinates struggles to represent sharp gradients, boundary layers, and other non-periodic structures commonly found in PDEs posed on bounded domains with Dirichlet or Neumann boundary conditions. To address these limitations, we introduce the Spectral-Embedded DeepONet (SEDONet), a new DeepONet variant in which the trunk is driven by a fixed Chebyshev spectral dictionary rather than coordinate inputs. This non-periodic spectral embedding provides a principled inductive bias tailored to bounded domains, enabling the learned operator to capture fine-scale non-periodic features that are difficult for Fourier-based or MLP-only trunks to represent. SEDONet is evaluated on a suite of PDE benchmarks including 2-D Poisson, 1-D Burgers, 1-D Advection-Diffusion, Allen-Cahn dynamics, and the Lorenz-96 chaotic system covering elliptic, parabolic, advective, and multiscale temporal phenomena, all of which can be viewed as canonical problems in computational mechanics. Across all datasets, SEDONet consistently achieves the lowest relative  $\ell_2$  errors among DeepONet, FEDONet, and SEDONet, with average improvements of 30-40% over the baseline DeepONet and meaningful gains over Fourier-embedded variants on non-periodic geometries. Spectral analyses further show that SEDONet more accurately preserves high-frequency and boundary-localized features, demonstrating the value of Chebyshev embeddings in non-periodic operator learning. The proposed architecture offers a simple, parameter-neutral modification to DeepONets, delivering a robust and efficient spectral framework for surrogate modeling of PDEs on bounded domains.

**Keywords:** Scientific Machine Learning (SciML); Neural Operator Learning; Chebyshev spectral embeddings; Deep Operator Networks; Partial Differential Equations.

## 1 Introduction

Partial differential equations (PDEs) serve as the foundation for modelling a wide range of physical, biological and engineering systems, including diffusion, transport, turbulence, phase transitions and chaotic dynamics. Classical numerical methods, finite-difference, finite-element, and spectral discretizations, provide high-fidelity solutions but are computationally expensive when repeatedly solving parametric or high-dimensional PDEs, or when rapid surrogate evaluations are required [1–3]. To accelerate PDE modelling pipelines, a long line of research has investigated surrogate approximations, including universal neural approximators [4–7], reduced-order models such as POD [8, 9], Gaussian process regression [10], and mesh-free radial-basis approaches [11, 12]. While successful on fixed grids, these classical surrogates do not naturally extend to operator learning, the task of learning mappings between infinite-dimensional function spaces.

Neural operators address this challenge by learning solution operators directly from data. Deep Operator Networks (DeepONets) [13] and Neural Operators [14] define branch-trunk factorizations that generalise across discretisations and provide operator-level universal approximation guarantees. Fourier Neural Operators (FNOs) extend this idea

using global spectral convolutions and have demonstrated strong performance on fluid and parametric PDEs [15]. Subsequent variants integrate multi-wavelets [16, 17], hierarchical tensorisation [18, 19], graph kernels [20, 21], and geometry-aware deformations [22–24], further enriching the operator-learning landscape. Recent work has also emphasised closure modelling and multifidelity formulations in multiscale settings, notably the multifidelity DeepONet approaches of Ahmed and Stinis and co-workers [25, 26]. Kernel and Gaussian-process baselines have been revisited in this context, showing that carefully designed kernel methods can be competitive with neural operators [27] and that neural-operator-induced Gaussian processes provide a probabilistic, uncertainty-aware extension of deterministic operators [28].

Beyond these foundational architectures, operator learning has recently expanded toward more specialized and physically informed formulations. New directions include neuroscience-inspired neural operators that strengthen multiscale feature representation [29], derivative-informed architectures that embed local sensitivity structure [30], and methods designed to mitigate spectral bias in stiff or multiscale PDE regimes [31]. Other developments target challenging physical settings such as interface-dominated problems, where interface-aware operator networks improve discontinuity resolution [32, 33], and scenarios involving geometric or resolution variability, where local and resolution-invariant operator formulations enhance generalization across meshes and spatial discretizations [34, 35]. Complementary research leverages dynamical-systems structure through Koopman-based operator-learning models [36], while nonlocal material behaviour has motivated peridynamic operator networks [37]. Additional work explores feature-adjacent mappings to stabilize learning in heterogeneous environments [38]. Together these advances illustrate a clear shift toward domain-informed, physics-aware neural operators that better capture complex PDE phenomena and broaden the applicability of operator-learning frameworks.

A rich body of work has further explored specialized neural operators for complex physical phenomena and non-standard constitutive behaviour. Peridynamic neural operators provide nonlocal constitutive models for material deformation [39], while probabilistic closure models combining conditional diffusion processes with neural operators have been proposed for stochastic turbulence modeling [40]. Resolution-independent neural operators [41] and local neural operators [42] address mesh and domain-variability, enabling robust generalization across resolutions and geometries. Physics-informed geometry-aware neural operators [43] and Cole–Hopf-based operator constructions [44] continue to illustrate how classical analytical transformations can enhance neural operator architectures.

In parallel, there has been rapid progress in physics-informed and probabilistic operator learning. Physics-informed DeepONets and neural operators [45–48] incorporate PDE residuals and variational principles into the training objective, while latent neural operators and invertible Fourier neural operators introduce expressive latent spaces and reversible dynamics [49–52]. Sobolev-style training strategies [53] and unsupervised operator learning for mean-field games [54] highlight the role of derivative information and weak formulations in improving generalization. At the same time, in-context generalization properties of operator networks are being explored through PDE-oriented in-context models [55]. Collectively, these developments indicate a maturing ecosystem where neural operators, Gaussian processes, and hybrid architectures are increasingly unified.

Despite these advances, the trunk network in DeepONet, responsible for encoding spatial or spatiotemporal coordinates, is typically a shallow multilayer perceptron (MLP). MLPs exhibit a well-known spectral bias, that preferentially learn low-frequency components while struggling with high-frequency, oscillatory or multiscale patterns [56]. This significantly affects PDEs with boundary layers, steep gradients, or sharp phase-field transitions. In Euclidean neural networks, this issue is often mitigated by positional encodings such as sinusoidal/Fourier features [57] or learned embeddings [58]. In particular, Fourier-Embedded DeepONet (FEDONet) [59] incorporates Fourier features into DeepONet trunks, improving performance on periodic or nearly periodic PDEs. However, Fourier features encode a fundamentally periodic prior and are therefore less suited to bounded, non-periodic domains common in elliptic and parabolic PDEs, motivating alternative non-periodic or polynomial spectral priors such as those explored in [41, 42, 60].

Chebyshev polynomials provide an orthogonal basis on bounded intervals and form the cornerstone of polynomial spectral methods [1, 2]. They offer exponential convergence for smooth solutions, excellent resolution of boundary layers, and natural compatibility with non-periodic boundary conditions. A growing literature explores Chebyshev-based neural representations, including Chebyshev neural networks [61], fractional PDE solvers [62], Chebyshev spectral neural networks [63], orthogonal polynomial neural operators [60], Chebyshev-enhanced PINNs [64, 65], hybrid Chebyshev–attention architectures [66], and Chebyshev feature networks [67]. Spectral neural operators combining Fourier and Chebyshev representations have also been proposed [68]. These studies suggest that embedding Chebyshev structure inside modern neural PDE solvers can substantially improve stability and accuracy on non-periodic domains.

However, existing Chebyshev-based neural architectures either parametrize the solution directly in spectral space, or operate on coefficient maps rather than spatial coordinates. None provide a simple, drop-in non-periodic spectral

embedding for DeepONet trunks analogous to Fourier embeddings in FEDONet. To bridge this gap, we propose the Spectral-Embedded DeepONet (SEDONet), a Chebyshev-based operator network in which raw coordinates are replaced by a fixed tensor-product Chebyshev embedding. The embedding supplies a structured polynomial basis aligned with bounded, non-periodic domains. The branch network remains unchanged, while the trunk network mixes Chebyshev modes into adaptive basis functions. SEDONet introduces no additional trainable parameters, preserves the DeepONet factorization, and is compatible with existing DeepONet/FEDONet implementations.

We evaluate SEDONet on the following five benchmark systems:

- 2-D Poisson equation (elliptic),
- 1-D viscous Burgers equation (nonlinear transport-diffusion),
- 1-D advection-diffusion equation (Dirichlet boundaries),
- Lorenz-96 chaotic ODE system, and
- Allen-Cahn phase-field equation (interface dynamics).

These benchmarks span elliptic, parabolic, stiff nonlinear, and chaotic systems, providing a broad testbed that includes boundary layers, shocks and phase transitions. Across all tasks, SEDONet achieves lower relative  $L^2$  error than DeepONet and matches or exceeds FEDONet, particularly on non-periodic PDEs. Our primary objective in this study is to examine Chebyshev-based spectral embeddings and to compare their performance against conventional Fourier embeddings.

Our work makes three primary contributions, those are summarized as follows: First, we introduce a Chebyshev-embedded trunk for DeepONet, providing a plug-and-play spectral coordinate embedding tailored to non-periodic PDE domains. This design preserves the original branch-trunk factorization while equipping the trunk with a principled polynomial spectral prior. Second, we provide a theoretical analysis showing that the resulting Chebyshev features form an approximately orthogonal and well-conditioned Gram matrix, thereby expanding the hypothesis class of coordinate-input DeepONets and improving their ability to represent functions with boundary layers or steep gradients. Third, through the extensive experiments on the five diverse benchmarks including elliptic, parabolic, nonlinear transport, chaotic ODE dynamics, and phase-field models, we demonstrate that SEDONet consistently improves reconstruction accuracy while maintaining discretizations invariance and low model complexity. Together, these developments embed the structure of classical non-periodic spectral methods directly into the trunk of DeepONet, extending operator learning beyond Fourier-based embeddings and offering a natural bridge between polynomial spectral approximation theory and modern neural operator architectures.

The remainder of this paper is organized as follows. Section 2 presents the formulation of the Spectral-Embedded DeepONet (SEDONet), detailing the Chebyshev spectral embedding, its integration into the trunk network, and the resulting spectral interpretation for operator approximation on bounded domains. Section 3 describes the benchmark setup, dataset generation, and implementation details across the five representative operator families considered, including elliptic, parabolic, advective-diffusive, chaotic, and phase-field dynamics. Section 4 reports the quantitative and qualitative results, highlighting the improvements achieved by SEDONet over DeepONet and FEDONet in reconstruction accuracy, boundary resolution, and spectral fidelity. Finally, Section 5 concludes the study and outlines several promising research directions in spectral operator learning, adaptive polynomial embeddings, and physics-informed neural operator architectures.

## 2 Methodology

### 2.1 Problem Formulation

We consider the problem of learning nonlinear operators between infinite-dimensional function spaces. Let  $\Omega \subset \mathbb{R}^D$  be a bounded domain, and define the input and output function spaces

$$\mathcal{U} = \{u : \mathcal{X} \rightarrow \mathbb{R}^{d_u}\}, \quad \mathcal{X} \subseteq \mathbb{R}^{d_x}, \quad (1)$$

$$\mathcal{S} = \{s : \mathcal{Y} \rightarrow \mathbb{R}^{d_s}\}, \quad \mathcal{Y} \subseteq \mathbb{R}^{d_y}. \quad (2)$$

We assume access to paired samples  $\mathcal{D} = \{(u^i, s^i)\}_{i=1}^N$  from an unknown operator  $\mathcal{G} : \mathcal{U} \rightarrow \mathcal{S}$ , e.g., the solution operator of a PDE mapping initial or forcing data to a full space-time field. Our goal is to learn a parametric approximation  $\mathcal{G}_\theta : \mathcal{U} \rightarrow \mathcal{S}$  that generalizes to new, unseen functions  $u \in \mathcal{U}$ .

Deep Operator Networks (DeepONets) provide a natural architecture for this task. Each prediction decomposes into a branch-trunk factorization of the form

$$\mathcal{G}_\theta(u)(\zeta) = B_\theta(u) \cdot T_\theta(\zeta), \quad \zeta = (x, y, z, t), \quad (3)$$

where the branch network  $B_\theta$  encodes discrete samples of the input function  $u$  and the trunk network  $T_\theta$  encodes coordinate queries  $\zeta$ . This separation mirrors classical spectral representations: the branch returns coefficients, while the trunk returns basis functions evaluated at  $\zeta$ . Consequently, the choice of trunk representation is crucial for the model’s spectral expressivity and its ability to represent different PDE structures.

## 2.2 Spectral Embeddings for Non-Periodic Operators

In the standard DeepONet formulation,  $T_\theta(\zeta)$  is produced by a multi-layer perceptron (MLP) acting directly on the raw coordinates. This simple parameterization is universal in principle, but in practice it exhibits a strong spectral bias toward low frequencies and often struggles with non-periodic geometries, sharp gradients, and boundary layers. Coordinate encodings based on sinusoidal features (e.g., Fourier features or positional embeddings) can partially alleviate this issue, but they are most naturally tailored to periodic domains.

Many operators arising in scientific computing are instead defined on bounded intervals with Dirichlet or Neumann boundary conditions. Examples include elliptic Poisson problems, reaction-diffusion systems, advective-diffusive flows, and chaotic ODEs (when interpreted as operators on a finite time window). For such settings, polynomial spectral methods, in particular Chebyshev expansions, provide well-conditioned, rapidly convergent bases on  $[-1, 1]$  that naturally resolve boundary layers and steep gradients.

These observations motivate a trunk architecture that embeds coordinates into a non-periodic spectral dictionary before applying a learned MLP. The resulting model, which we call the Spectral-Embedded DeepONet (SEDONet), combines the flexibility of DeepONets with the approximation properties of Chebyshev spectral methods.

## 2.3 Spectral-Embedded DeepONet (SEDONet): Chebyshev Trunk for Bounded Domains

SEDONet retains the classical DeepONet branch but augments the trunk with a deterministic Chebyshev polynomial dictionary. Instead of feeding raw coordinates to the trunk MLP, we first compute fixed spectral features

$$\phi_{\text{Cheb}}(y) \in \mathbb{R}^{d_{\text{trunk}}}, \quad y = (x, t), \quad (4)$$

and then learn a nonlinear mapping from these features to trunk outputs. The resulting model can be interpreted as a data-driven Chebyshev expansion adapted to bounded, non-periodic PDE domains.

In one-dimensional Chebyshev basis, for a spatial coordinate  $x \in [0, 1]$ , we apply the affine transformation

$$\xi = 2x - 1 \in [-1, 1], \quad (5)$$

and work with the standard Chebyshev polynomials of the first kind  $\{T_n\}_{n \geq 0}$  defined by the recurrence

$$T_0(\xi) = 1, \quad T_1(\xi) = \xi, \quad T_{n+1}(\xi) = 2\xi T_n(\xi) - T_{n-1}(\xi). \quad (6)$$

These polynomials form an orthogonal basis on  $[-1, 1]$  with respect to the weight  $w(\xi) = (1 - \xi^2)^{-1/2}$  (see Appendix A for details). Orthogonality and the clustering of Chebyshev nodes near the endpoints make this basis particularly effective for representing non-periodic PDE solutions with boundary layers and steep gradients.

In the tensor-product spectral dictionary, for spatio-temporal inputs  $y = (x, t) \in [0, 1]^2$ , we map

$$\xi_x = 2x - 1, \quad \xi_t = 2t - 1, \quad (7)$$

and construct a tensor-product dictionary as follows

$$\Phi_{ij}(x, t) = T_i(\xi_x) T_j(\xi_t), \quad 0 \leq i < K_x, \quad 0 \leq j < K_t. \quad (8)$$

Collecting all entries in lexicographic order yields the full deterministic feature vector of the following form as

$$\Phi_{\text{full}}(x, t) = [\Phi_{00}, \Phi_{01}, \dots, \Phi_{K_x-1, K_t-1}]^\top \in \mathbb{R}^{K_x K_t}. \quad (9)$$

This tensor-product construction extends immediately to higher spatial dimensions by adding additional Chebyshev factors.

For the fixed-width Chebyshev embedding, the common practice, the trunk network expects a fixed input dimension  $d_{\text{trunk}}$  that may differ from  $K_x K_t$ . To bridge this gap we introduce a simple crop/pad operator  $C : \mathbb{R}^{K_x K_t} \rightarrow \mathbb{R}^{d_{\text{trunk}}}$  and define the final embedding as

$$\phi_{\text{Cheb}}(x, t) = C \Phi_{\text{full}}(x, t). \quad (10)$$

The operator  $\mathcal{C}$  can either truncate higher-order modes or pad with zeros, depending on the chosen spectral resolution. Importantly,  $\phi_{\text{Cheb}}$  is deterministic and fixed, no trainable parameters are attached to the embedding itself, so the inductive spectral structure remains stable during optimization.

For the trunk network, the SEDONet trunk maps Chebyshev features to  $p$  latent basis channels as the followings

$$T_\theta(x, t) = \Psi_\theta(\phi_{\text{Cheb}}(x, t)) = [t_1(x, t), \dots, t_p(x, t)]^\top \in \mathbb{R}^p, \quad (11)$$

where  $\Psi_\theta$  is an MLP. The functions  $t_k(x, t)$  can be viewed as learned basis functions formed by nonlinear modulation of Chebyshev modes.

In the branch network and operator synthesis, the branch network mirrors the standard DeepONet branch. Given discrete samples of an input function  $u_0$ , it produces latent coefficients

$$B_\theta(u_0) = [b_1(u_0), \dots, b_p(u_0)]^\top. \quad (12)$$

The predicted solution at any coordinate  $(x, t)$  is then synthesized via the DeepONet rule as followings

$$\hat{u}(x, t; u_0) = B_\theta(u_0)^\top T_\theta(x, t) = \sum_{k=1}^p b_k(u_0) t_k(x, t). \quad (13)$$

This expression highlights the analogy with classical spectral methods, the branch computes generalized ‘‘spectral coefficients’’ from  $u_0$ , while the trunk provides basis functions evaluated at  $(x, t)$ . For the training objective, given training pairs  $(u_0^{(i)}, u^{(i)})$  evaluated at points  $\{(x^q, t^q)\}_{q=1}^Q$ , we train SEDONet by minimizing the empirical mean-squared error as follows

$$\mathcal{L}_{\text{SEDONet}}(\theta) = \frac{1}{NQ} \sum_{i=1}^N \sum_{q=1}^Q |B_\theta(u_0^{(i)})^\top T_\theta(x^q, t^q) - u^{(i)}(x^q, t^q)|^2. \quad (14)$$

We employ mini-batch Adam optimization. All trainable parameters reside in the branch and trunk MLPs; the Chebyshev embedding is fixed and non-learnable, acting purely as an inductive bias. For the spectral interpretation, it is convenient to view SEDONet in a spectral framework. Suppose the trunk and branch can be written as

$$T_\theta(x, t) = [\psi_1(x, t), \dots, \psi_p(x, t)]^\top, \quad B_\theta(u_0) = [\langle u_0, \varphi_1 \rangle, \dots, \langle u_0, \varphi_p \rangle]^\top,$$

for some learned feature functionals  $\varphi_k$  and also the basis functions  $\psi_k$ . Then the prediction admits the form as

$$\hat{\mathcal{G}}(u_0)(x, t) \approx \sum_{k=1}^p \langle u_0, \varphi_k \rangle \psi_k(x, t), \quad (15)$$

i.e., a data-driven Chebyshev-type spectral expansion. Compared to vanilla coordinate-input trunks, the hypothesis space induced by Chebyshev embeddings strictly enlarges the class of representable functions on bounded domains (see Appendix B).

## 2.4 Training and Evaluation Protocol

After defining the architecture, we train SEDONet, DeepONet, and FEDONet under a common protocol and compare their performance on five benchmark families including 2-D Poisson, 1-D Burgers, 1-D advection-diffusion, Allen-Cahn, and Lorenz-96. During training, each mini-batch consists of a set of input functions  $\{u_0^{(i)}\}$  and corresponding reference solutions  $\{u^{(i)}(x^q, t^q)\}$  sampled on dense grids. For each architecture, we compute the branch coefficients, trunk outputs, and synthesized predictions via (13), and update parameters by minimizing the loss (14) (or its DeepONet/FEDONet counterparts). On held-out test data, we use several complementary diagnostics, for a given test input  $u$ , we evaluate the relative  $\ell_2$  error as

$$\varepsilon_{L^2}(u) = \frac{\|\mathcal{G}_\theta(u) - \mathcal{G}(u)\|_2}{\|\mathcal{G}(u)\|_2}, \quad (16)$$

computed on a dense evaluation grid tailored to each benchmark. This metric quantifies the normalized discrepancy between the reference and predicted fields, and forms the basis of the summary statistics reported in Table 1 and the error-bar plots. For the spectral fidelity for PDE benchmarks, we additionally compute angle-integrated power spectra of the reference and predicted solutions and compare  $E_{\text{pred}}(k)$  to  $E_{\text{ref}}(k)$ . This reveals how well each architecture captures multiscale structure and high-frequency content, beyond what is visible in a single scalar error.

Finally, for the qualitative diagnostics, we visualize representative solution fields and corresponding error maps. These plots highlight model behavior near boundaries, interfaces, and nonlinear structures where baseline methods are known to deteriorate. The qualitative observations are reported in Section 3 and closely track the quantitative trends. This unified protocol enables a fair comparison of spectral resolution, boundary behavior, and generalization performance across all three operator-learning architectures.

## 2.5 Algorithmic Workflow

The learning procedure for SEDONet follows the general DeepONet framework but replaces raw coordinate inputs with the Chebyshev spectral embedding introduced in Section 2.3. This results in a branch-trunk architecture in which the branch network encodes the input function  $u_0$ , and the trunk network evaluates Chebyshev-modulated basis functions at any spatio-temporal coordinate  $(x, t)$ . Figure 1 provides a schematic overview of this structure, illustrating how the branch and trunk outputs are combined through an inner product to produce operator evaluations.

---

**Algorithm 1** Training procedure for SEDONet
 

---

**Require:** Training set  $\mathcal{D} = \{(u_0^{(i)}, u^{(i)})\}_{i=1}^N$ , coordinate grid  $\{(x^q, t^q)\}_{q=1}^Q$ , number of trunk channels  $p$ , learning rate  $\eta$ , number of epochs  $E$

**Ensure:** Trained parameters  $\theta = (\theta_{\text{branch}}, \theta_{\text{trunk}})$

- 1: Initialize  $\theta_{\text{branch}}, \theta_{\text{trunk}}$
- 2: **for**  $e = 1, \dots, E$  **do**
- 3:   **for** each mini-batch  $\mathcal{B} \subset \mathcal{D}$  **do**
- 4:     Sample input functions  $\{u_0^{(i)}\}_{i \in \mathcal{B}}$  and reference values  $\{u^{(i)}(x^q, t^q)\}_{i \in \mathcal{B}, q=1, \dots, Q}$
- 5:     **Branch step:** compute latent coefficients  $B_\theta(u_0^{(i)}) \in \mathbb{R}^p$  for all  $i$
- 6:     **Trunk step:** for each grid point  $(x^q, t^q)$ , evaluate Chebyshev embedding  $\phi_{\text{Cheb}}(x^q, t^q)$  and trunk output  $T_\theta(x^q, t^q) \in \mathbb{R}^p$
- 7:     **Synthesis:** form predictions  $\hat{u}^{(i)}(x^q, t^q) = B_\theta(u_0^{(i)})^\top T_\theta(x^q, t^q)$
- 8:     **Loss:** compute  $\mathcal{L}_{\text{SEDONet}}(\theta)$  using (14)
- 9:     **Update:** apply one Adam step with learning rate  $\eta$  to update  $\theta_{\text{branch}}, \theta_{\text{trunk}}$
- 10:   **end for**
- 11: **end for**

---

During training, SEDONet alternates between three stages for each mini-batch. Firstly, encoding the input function through the branch net to obtain latent coefficients, then secondly evaluating the Chebyshev embedding and trunk net at all query points, and lastly synthesizing predictions by contracting the branch and trunk outputs, followed by gradient-based parameter updates. Because the Chebyshev embedding is fixed, the trunk network receives a stable spectral dictionary, which improves conditioning and accelerates convergence compared to purely coordinate-based trunks. Algorithm 1 provides a detailed summary of this workflow.

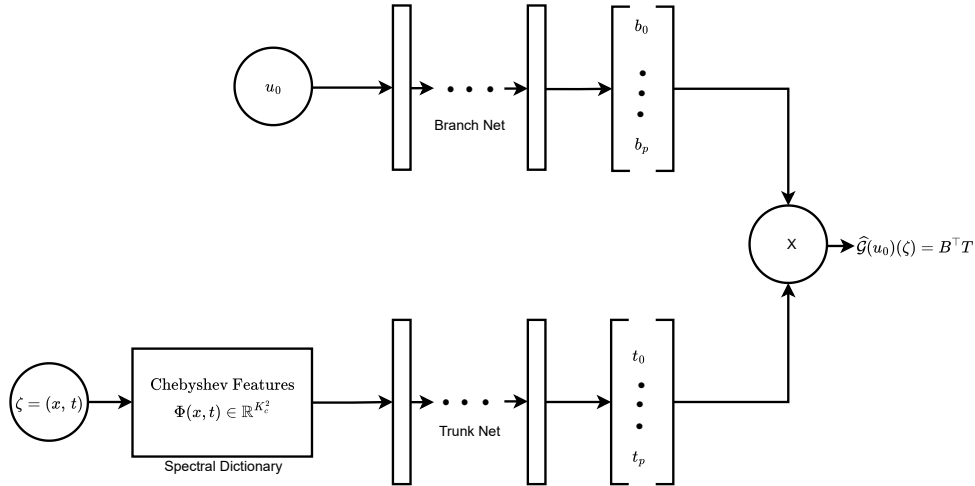


Figure 1: **SEDONet architecture:** The branch network maps discrete samples of the input function  $u_0$  to latent coefficients  $b_k$ , while the trunk network maps Chebyshev spectral features  $\Phi(x, t)$  to basis channels  $t_k(x, t)$ . Their inner product yields the operator evaluation  $\hat{\mathcal{G}}(u_0)(x, t)$ .

As illustrated in Figure 1, the division of labour between the branch and trunk networks results in a flexible yet structured operator-learning pipeline. The branch network captures the dependence of the solution on the input function, while the Chebyshev-enhanced trunk network provides a spectrally rich representation of the output domain. This separation enables SEDONet to generalize across discretizations and spatial resolutions while retaining the favorable approximation properties of Chebyshev spectral methods on bounded, non-periodic domains.

### 3 Results

#### 3.1 2D Poisson Equation

We evaluate all three models, DeepONet, FEDONet, and the proposed SEDONet, on the two-dimensional Poisson equation

$$\nabla^2 u(x, y) = f(x, y), \quad (x, y) \in [0, 1]^2, \quad (17)$$

subject to homogeneous Dirichlet boundary conditions,

$$u(x, y)|_{\partial\Omega} = 0. \quad (18)$$

The forcing field  $f(x, y)$  serves as input, and  $u(x, y)$  denotes the steady-state solution. A dataset of  $N = 10,000$  operator pairs is constructed by sampling forcing fields from a Gaussian Random Field,

$$f \sim \text{GRF}(\alpha = 3, \tau = 3),$$

on a uniform  $128 \times 128$  grid and solving the Poisson problem using a five-point finite-difference discretization. This yields the linear system

$$A\mathbf{u} = \mathbf{b},$$

where  $\mathbf{b}$  is the vectorized forcing and  $\mathbf{u}$  is the numerical solution. The matrix  $A$  follows the standard discrete Laplacian stencil,

$$A_{ij} = \begin{cases} 4, & i = j, \\ -1, & \text{if nodes } i \text{ and } j \text{ share an edge,} \\ 0, & \text{otherwise,} \end{cases}$$

with boundary rows modified to impose the homogeneous Dirichlet conditions.

Figure 2 presents a representative test example. The left panel displays the input forcing field, followed by the exact solution and the predictions from DeepONet, FEDONet, and SEDONet, together with their pointwise residual fields. DeepONet captures the overall structure but exhibits smoothing of interior features and larger residual magnitudes. FEDONet improves spatial fidelity through Fourier embeddings, though its sinusoidal basis is not naturally aligned with non-periodic boundaries. SEDONet achieves the most accurate reconstruction: its Chebyshev-based spectral embedding aligns well with bounded domains, enabling it to resolve both interior variations and boundary gradients more effectively. Its residual field displays the lowest amplitude and smoothest spatial structure among the three models.

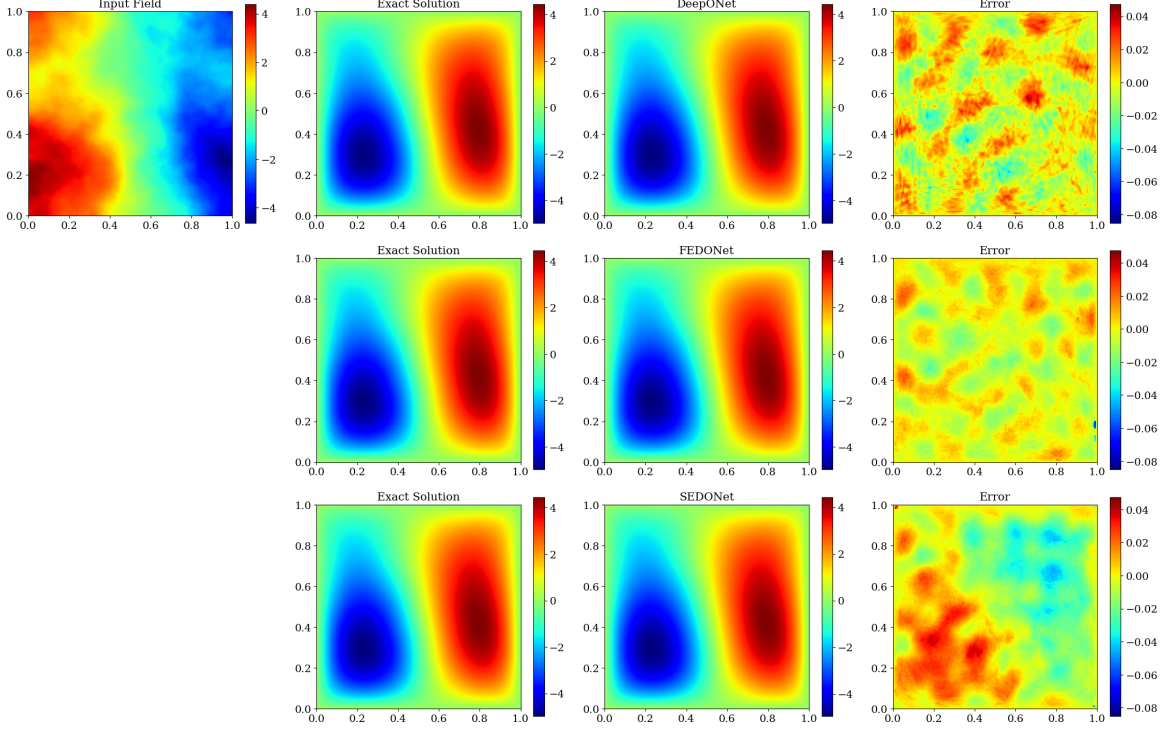


Figure 2: Comparison of DeepONet, FEDONet, and SEDONet on a representative test example from the 2D Poisson dataset. The left panel shows the forcing field; the remaining panels show the exact solution, model predictions, and the corresponding pointwise residual fields.

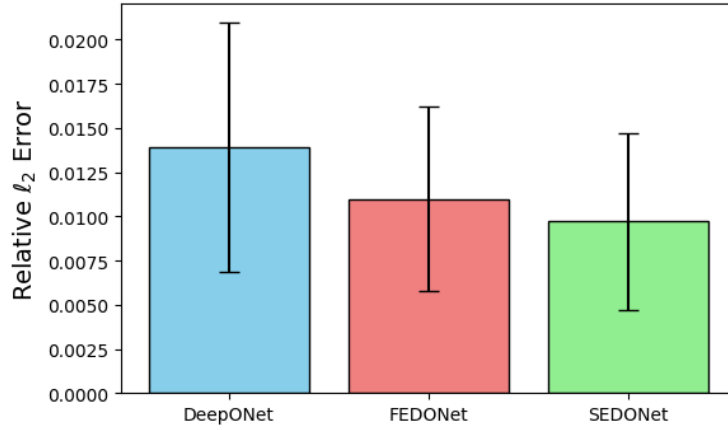


Figure 3: Relative  $\ell_2$  error (mean  $\pm$  std) across 1000 unseen Poisson test set for all three architectures. SEDONet achieves both the lowest mean error and the lowest variance.

These qualitative observations are consistent with the quantitative results. Across the full test set, DeepONet attains a mean relative  $\ell_2$  error of 1.39%, FEDONet reduces this to 1.10%, and SEDONet further improves the accuracy to **0.97%**. This corresponds to improvements of 31.2% over DeepONet and 11.0% over FEDONet. The bar plot in Figure 3 summarizes these results and shows both the mean errors and their standard deviations, highlighting the improved accuracy and consistency achieved by SEDONet.



### 3.2 Burger’s Equation

We evaluate the three operator-learning architectures on the one-dimensional viscous Burger’s equation defined on a bounded, non-periodic domain. The governing PDE is

$$\frac{\partial u}{\partial t}(x, t) + u(x, t) \frac{\partial u}{\partial x}(x, t) = \nu \frac{\partial^2 u}{\partial x^2}(x, t), \quad (x, t) \in [0, 1] \times [0, T], \quad (19)$$

with viscosity  $\nu = 0.01$  and final time  $T = 0.3$ . Unlike periodic benchmark settings, we impose homogeneous Dirichlet boundary conditions,

$$u(0, t) = 0, \quad u(1, t) = 0, \quad (20)$$

which introduce boundary layers that are not naturally aligned with Fourier-based representations.

To generate a diverse family of smooth initial conditions, we sample a random superposition of sine modes,

$$u(x, 0) = c_1 \sin(\pi x) + c_2 \sin(2\pi x) + c_3 \sin(3\pi x), \quad (21)$$

where  $c_1, c_2, c_3 \sim \mathcal{N}(0, 0.3^2)$ . Each realization is evolved numerically using a stable explicit finite-difference scheme with upwind discretization of the advective term and centered stencils for diffusion. Trajectories exhibiting numerical instabilities (NaNs or  $\|u\|_\infty > 5$ ) are discarded and resampled. This procedure yields a final dataset of 1250 stable space-time solutions on a grid of  $N_x = N_t = 100$  points.

The learning task is to approximate the nonlinear operator

$$\mathcal{G} : u_0(x) \mapsto u(x, t), \quad (22)$$

mapping each initial state to its full temporal evolution. This provides a natural testbed for comparing DeepONet, FEDONet, and the proposed SEDONet under non-periodic conditions where Chebyshev embeddings are expected to offer an advantage. Figure 4 reports the relative  $\ell_2$  error over 128 unseen test samples. DeepONet exhibits the highest error (6.19%), followed by FEDONet (4.47%), while SEDONet achieves the lowest mean error at **3.98%**, reflecting its ability to better resolve boundary-layer dynamics and non-periodic structures.

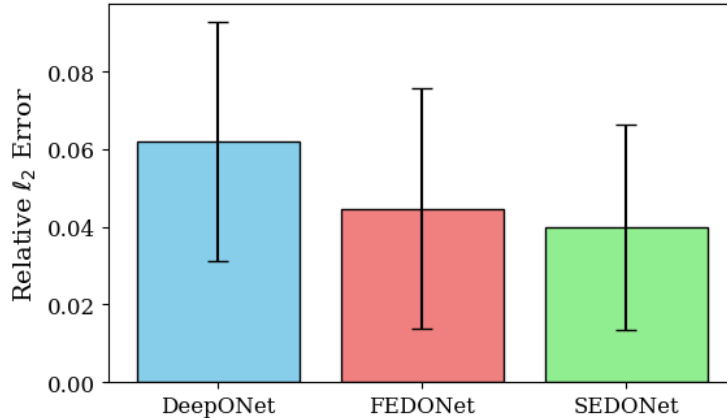


Figure 4: Relative  $\ell_2$  error across 128 unseen Burgers’ test samples for all three architectures (DeepONet, FEDONet, and SEDONet).

We can see that a test example is shown in Figure 5, that shows that DeepONet reconstructs only the coarse dynamics and visibly smooths the steep gradients. While the FEDONet improves this behavior but still struggles near sharp regions. Finally our proposed architecture SEDONet provides the closest match to the ground truth, accurately tracking gradient steepening and advective transport without introducing any kind of oscillations or excessive smoothing.

Spectral plot investigations in Figure 6 further highlight the performance gap, that show that DeepONet underestimates high-wavenumber energy, indicative of its spectral bias toward smooth, low-frequency reconstructions. Also, FEDONet partially mitigates this effect through Fourier embeddings but remains limited by the non-periodic domain. Finally,

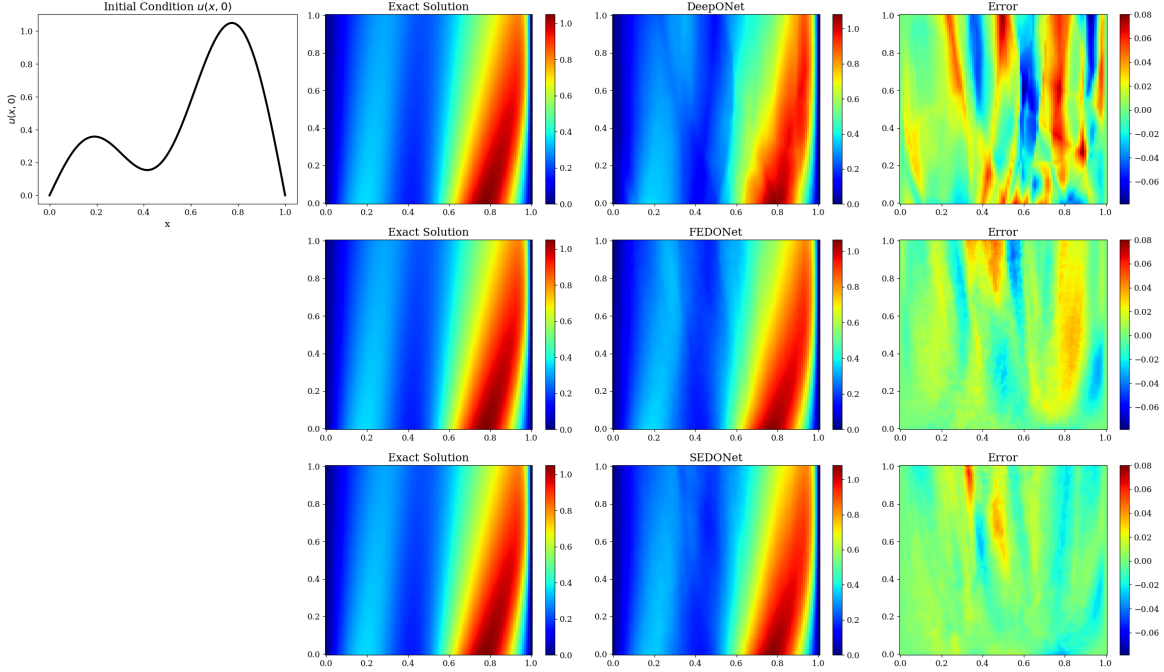


Figure 5: Best-performing Burgers' test sample: Ground truth, DeepONet, FEDONet, and SEDONet predictions with error maps.

SEDONet shows the closest agreement with the exact energy spectrum throughout the dissipative range, demonstrating that Chebyshev-based embeddings provides a more appropriate basis for operator learning on bounded intervals.

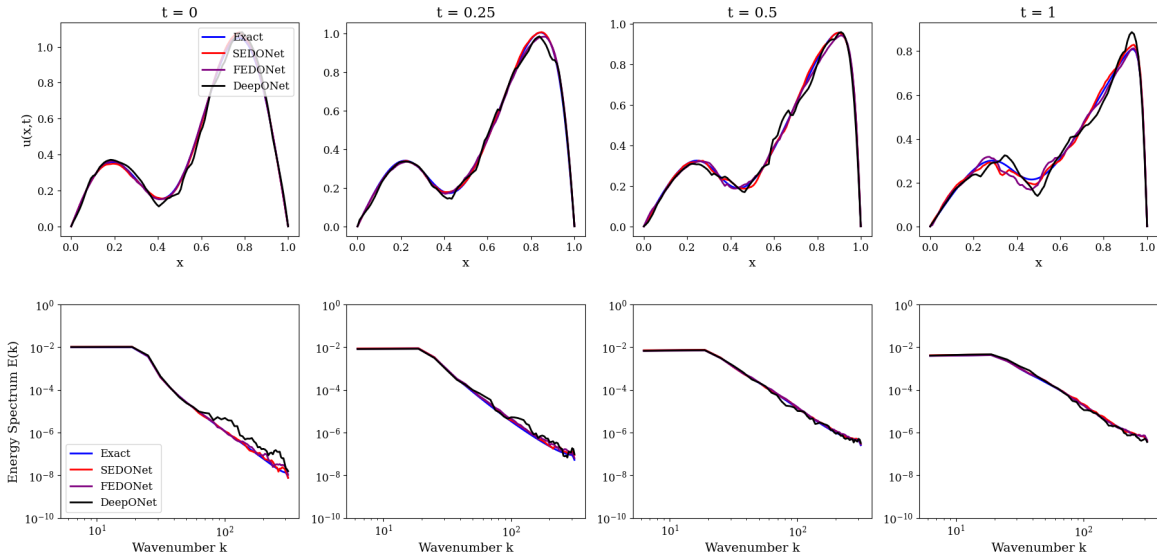


Figure 6: Energy spectrum comparison for Burgers' equation: temporal evolution of  $u(x, t)$  and corresponding spectral decay for DeepONet, FEDONet, and SEDONet.

Overall, the Burgers' experiments confirm that SEDONet provides a stronger inductive bias for non-periodic PDEs than both DeepONet and FEDONet. Its improved boundary handling, sharper spatial reconstructions, and more accurate spectral behavior collectively demonstrate the value of Chebyshev spectral embeddings in non-periodic operator learning.

### 3.3 Advection-Diffusion Equation

We next evaluate the models on the one-dimensional advection–diffusion equation posed on a strictly non-periodic domain:

$$u_t + c u_x = \nu u_{xx}, \quad x \in [0, 1], \quad t \in [0, T], \quad (23)$$

subject to homogeneous Dirichlet boundary conditions,

$$u(0, t) = 0, \quad u(1, t) = 0. \quad (24)$$

This setting reflects boundary-driven transport-diffusion processes common in physics and engineering, and provides a natural test case for architectures designed to capture non-periodic structure. The parameters are chosen as  $c = 0.03$  and  $\nu = 0.01$ , corresponding to a diffusion-dominated regime with  $Pe \approx 3$ . To construct a diverse set of initial states, each initial condition is formed from smooth, boundary-compatible components, including quadratic boundary-layer profiles and one or more interior Gaussian perturbations with random locations, widths, and amplitudes. All components vanish at the endpoints, ensuring that no periodic extension can represent the data and thus emphasizing the importance of non-periodic inductive biases in the trunk network.

The spatio-temporal dataset is generated using an explicit finite-difference solver in which the advection term is approximated by a first-order upwind stencil and the diffusion term by centered second differences. The time step is selected to satisfy the parabolic stability requirement  $\nu \frac{\Delta t}{\Delta x^2} \leq 0.5$ , ensuring stability for all trajectories. A total of 1250 stable simulations are produced, each consisting of an initial field  $u_0(x) \in \mathbb{R}^{100}$  and the full evolution  $u(t, x) \in \mathbb{R}^{100 \times 100}$ . Any trajectory exhibiting instability or unphysical magnitudes is automatically regenerated.

Figure 7 shows a representative test example comparing the exact solution with predictions from DeepONet, FEDONet, and SEDONet. DeepONet captures only the coarse dynamics, oversmoothing interior gradients and producing visible distortions near the boundaries. FEDONet improves upon this behavior, but its sinusoidal inductive bias introduces mild inaccuracies close to the Dirichlet boundaries where periodic structure is inappropriate. In contrast, SEDONet achieves the closest agreement with the exact solution throughout the entire spatio-temporal domain. The Chebyshev spectral embedding aligns naturally with the non-periodic geometry, enabling sharper representation of boundary layers and more accurate tracking of diffusive smoothing.

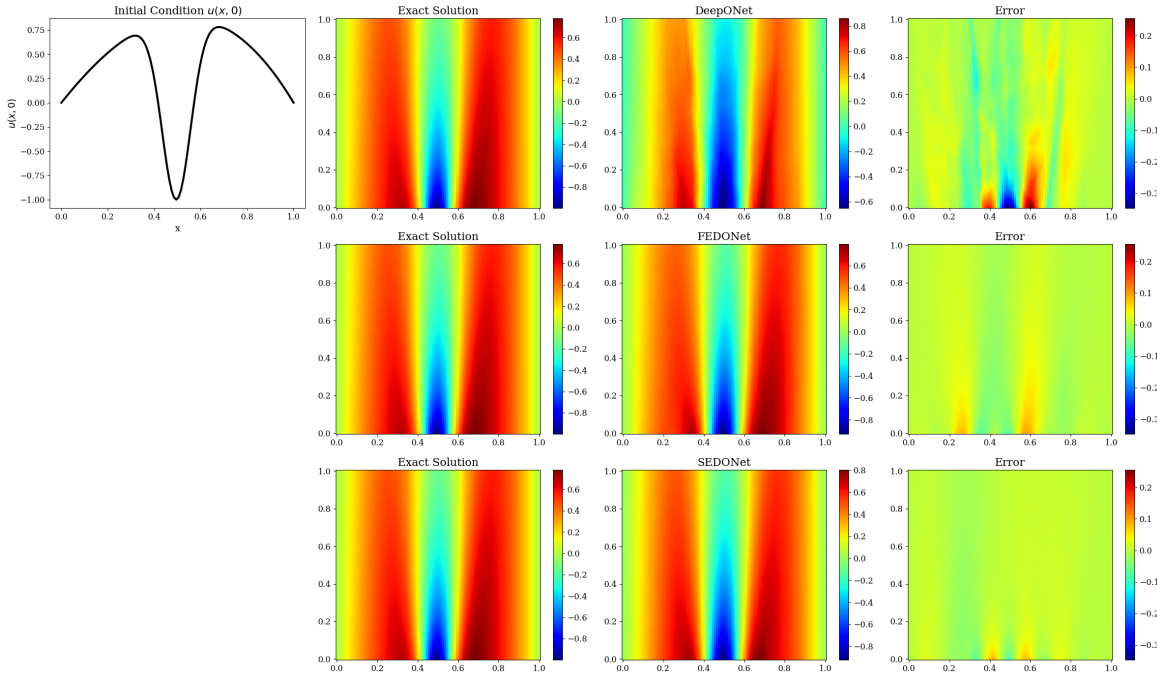


Figure 7: Representative test sample from the non-periodic advection-diffusion dataset. DeepONet exhibits smoothing and boundary distortion, FEDONet improves accuracy but retains mild periodic artifacts, and SEDONet provides the closest match to the exact solution across the full space-time domain.

These observations are consistent with the quantitative results. Across the full unseen test set, DeepONet yields an average relative  $\ell_2$  error of approximately 8.00%, FEDONet reduces this to 4.67%, and SEDONet further lowers

the error to about 4.33%. The bar plot in Figure 8, which displays both the mean and standard deviation across 250 independent test samples, confirms that SEDONet achieves the most accurate and most consistent performance among the three models.

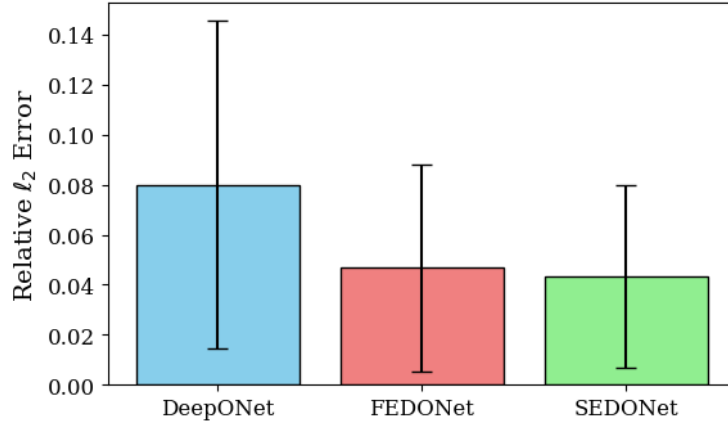


Figure 8: Relative  $\ell_2$  error (mean  $\pm$  std) across 250 unseen advection-diffusion test samples. SEDONet achieves the lowest error and improved robustness compared to both DeepONet and FEDONet.

Overall, this benchmark highlights that SEDONet provides a clear advantage when learning operators associated with non-periodic, boundary-constrained PDEs. The Chebyshev-based trunk offers a more suitable spectral representation than either the purely MLP-based DeepONet or the Fourier-based FEDONet, leading to improved fidelity in both physical structure and numerical accuracy.

### 3.4 Lorenz-96 Chaotic System

To further assess the generalization capabilities of neural operator architectures beyond PDEs, we evaluate DeepONet, FEDONet, and SEDONet on the Lorenz-96 (L96) model, a canonical benchmark in nonlinear dynamics, atmospheric modeling, and data assimilation. The governing equations are

$$\frac{dx_i}{dt} = (x_{i+1} - x_{i-2})x_{i-1} - x_i + F, \quad i = 1, \dots, N, \quad (25)$$

with periodic boundary conditions  $x_{i \pm N} = x_i$ . Here,  $x_i(t)$  denotes the  $i$ -th state variable, and the forcing parameter  $F$  controls the degree of nonlinearity. We set  $N = 40$  and  $F = 4.0$ , producing smooth but strongly nonlinear dynamics with coherent wave-like propagation. The system is integrated using a fourth-order Runge-Kutta (RK4) method with time step  $\Delta t = 0.01$ . Initial conditions are generated by perturbing the equilibrium state  $x_i = F$  with small Gaussian noise,  $\mathbf{x}_0 = F\mathbf{1} + \epsilon\mathcal{N}(0, I)$ ,  $\epsilon = 10^{-3}$ . Each trajectory is simulated for 15 seconds, where the initial 10 seconds are discarded to remove transients. The remaining 5 seconds form a sequence of 501 snapshots. Repeating this for 10,000 initial conditions produces a large ensemble of spatio-temporal trajectories with shape  $(10,000, 501, 40)$ .

Figure 9 shows representative test reconstructions. Each row includes the initial condition, the exact spatio-temporal evolution, predictions from DeepONet, FEDONet, and SEDONet, followed by the absolute error fields. All three models reproduce the dominant diagonal wave structures and maintain the phase velocity over the full prediction horizon. Vanilla DeepONet, however, shows mild phase drift and slight amplitude damping, especially in regions with sharper gradients. FEDONet alleviates some of these issues due to the Fourier-based positional encoding, though the improvement is modest because the Lorenz-96 attractor is inherently smooth.

SEDONet provides the most accurate long-horizon reconstruction. Its Chebyshev-based spectral trunk better regulates amplitude and reduces cumulative error, resulting in cleaner residual fields and smaller drift in regions where DeepONet and FEDONet deviate. This behavior is visible throughout the full spatio-temporal domain. These qualitative observations are further supported by the quantitative evaluation summarized in Figure 10. The bar plot displays the mean relative  $\ell_2$  error and associated standard deviation across 2000 unseen trajectories. DeepONet attains an average error of approximately 23.6%, FEDONet reduces this slightly to around 22.0%, and SEDONet further lowers the error to about 20.9%. In addition to having the lowest mean error, SEDONet also exhibits reduced variance, indicating more consistent performance across different initial conditions. Although the absolute improvements are smaller than those

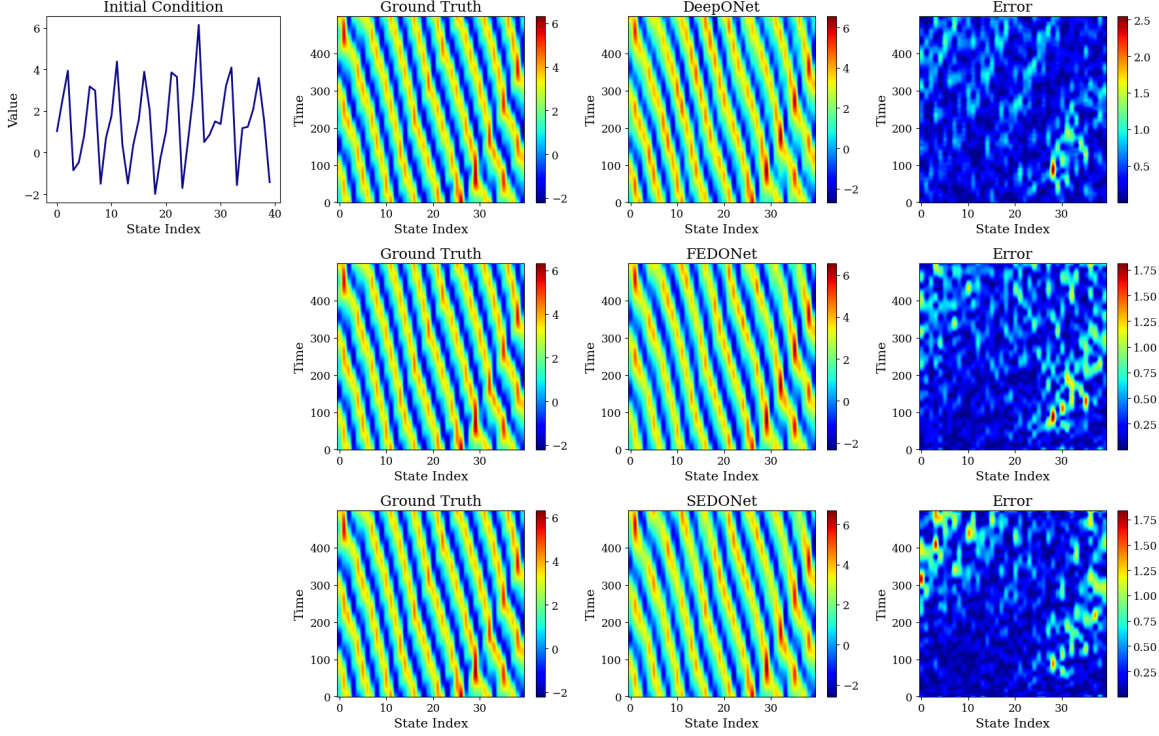


Figure 9: Spatio-temporal reconstruction of representative Lorenz-96 trajectories: ground truth, DeepONet, FEDONet, and SEDONet predictions, together with absolute error fields.

observed for elliptic or convection-diffusion PDEs, the trend remains robust, SEDONet achieves the best stability and predictive accuracy among the three architectures on long-horizon chaotic dynamics.

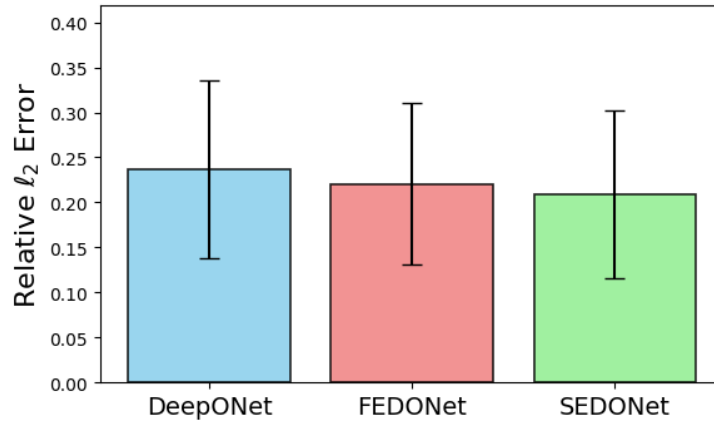


Figure 10: Relative  $l_2$  error (mean  $\pm$  std) across 2000 unseen Lorenz-96 trajectories. SEDONet achieves both the lowest average error and the lowest variance, demonstrating improved stability and robustness compared to DeepONet and FEDONet.

Overall, these results indicate that even for smooth, quasi-periodic systems like Lorenz-96, where fully connected trunks already perform reasonably well, the Chebyshev spectral embeddings of SEDONet still yield measurable benefits. The architecture improves stability, reduces phase and amplitude drift, and consistently achieves lower reconstruction error across thousands of independent trajectories.

### 3.5 Allen-Cahn Equation

We further benchmark the three operator-learning architectures on the one-dimensional Allen-Cahn equation, a nonlinear reaction-diffusion model describing phase separation and interface motion. The governing PDE is

$$\frac{\partial u}{\partial t} = \epsilon u_{xx} - 5u^3 + 5u, \quad x \in [-1, 1], \quad t \in [0, 1], \quad (26)$$

where  $u(x, t)$  is the phase-field variable and  $\epsilon = 10^{-4}$  controls the interface thickness. Periodic boundary conditions are imposed on both  $u$  and  $u_x$ , consistent with phase-field models on closed spatial domains. A dataset of 10,000 trajectories is generated using an explicit Euler integrator with spatial resolution  $\Delta x = 0.01$  and time step  $\Delta t = 0.005$ . The initial condition for each trajectory is constructed as

$$s(x) = \sum_{k=1}^3 \left[ a_k x^{2k} \cos(k\pi x) + b_k x^{2k} \sin(k\pi x) \right], \quad (27)$$

where  $a_k, b_k \sim \mathcal{U}(0, 1)$ . This yields sharply varying, multiscale profiles with strong spatial gradients, precisely the type of regime where spectral biases play a significant role. Each sample consists of the initial field  $s(x) \in \mathbb{R}^{200}$  and the full spatio-temporal solution  $u(x, t) \in \mathbb{R}^{200 \times 200}$ . The learning task is to approximate the nonlinear solution operator  $\mathcal{G} : s(x) \mapsto u(x, t)$ .

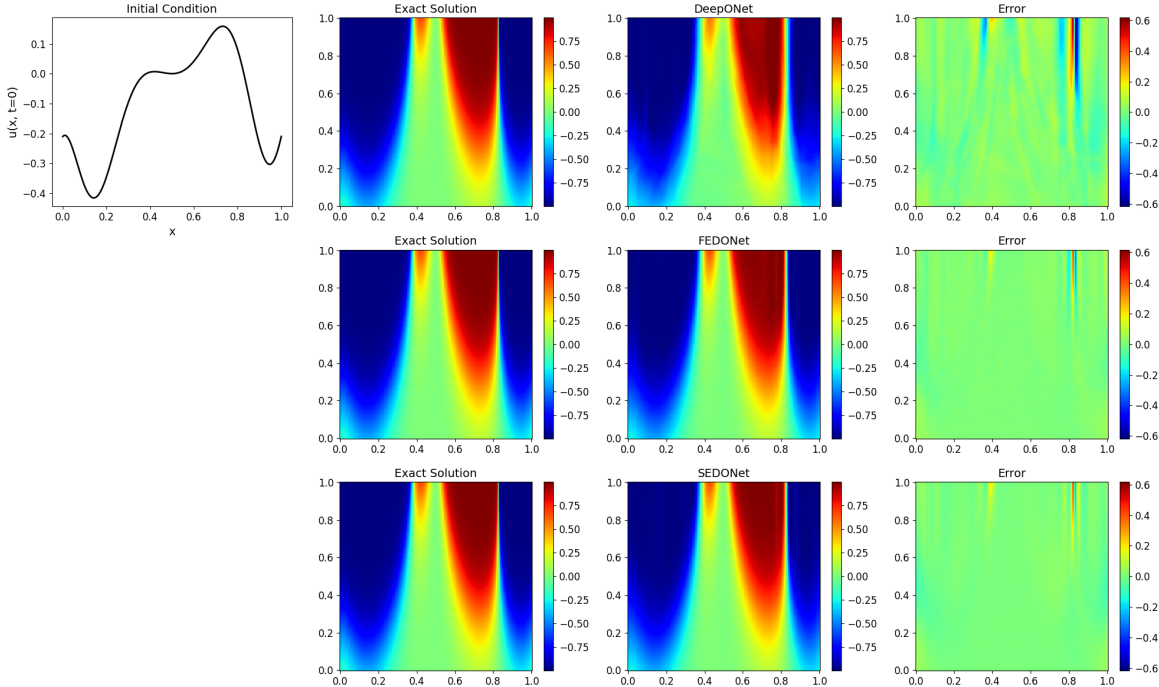


Figure 11: Spatio-temporal reconstruction for a representative Allen-Cahn test sample: ground truth, DeepONet, FEDONet, and SEDONet predictions, together with pointwise error fields.

Figure 11 presents a representative test example. DeepONet captures the broad temporal evolution but significantly blurs sharp phase interfaces, leading to visible misalignment during interface motion. FEDONet improves upon this behavior by preserving high-curvature regions and maintaining sharper transitions, yet mild smoothing remains in regions where steep gradients dominate.

SEDONet achieves the most accurate reconstruction among the three. Its Chebyshev-based spectral trunk aligns naturally with the polynomial and non-periodic structure of the initial data, enabling the model to preserve steep gradients and follow interface propagation with minimal artificial diffusion. The error fields show that SEDONet suppresses localized bursts of residual energy more effectively than both DeepONet and FEDONet, especially near thin interface layers where the cubic reaction term dominates the dynamics.



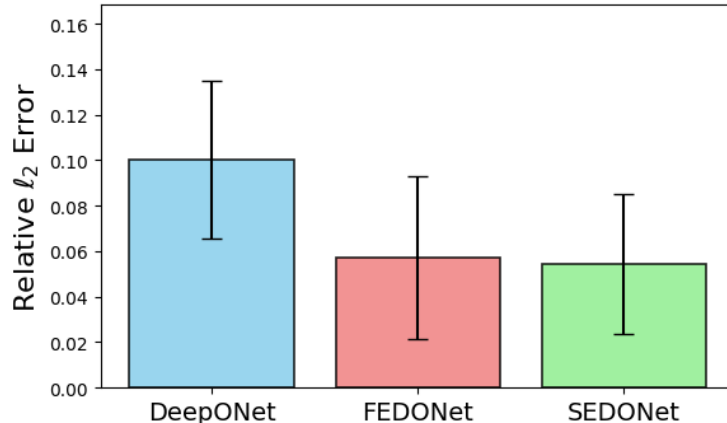


Figure 12: Relative  $\ell_2$  error (mean  $\pm$  std) across 250 unseen Allen-Cahn test samples for DeepONet, FEDONet, and SEDONet. SEDONet achieves the lowest error with reduced variance across the ensemble.

These qualitative observations are confirmed quantitatively by the results summarized in Figure 12. DeepONet yields the highest relative error at approximately 10.0%, FEDONet reduces this to around 5.7%, and SEDONet achieves the lowest error at roughly 5.4%. In addition to achieving the smallest mean error, SEDONet also exhibits slightly reduced variability compared to FEDONet, indicating more consistent performance across diverse initial conditions.

Overall, the Allen-Cahn benchmark demonstrates the advantage of domain-appropriate spectral embeddings when modeling nonlinear phase-field dynamics. While Fourier features enhance the representation of oscillatory structure, they can introduce mild ringing near steep gradients. In contrast, Chebyshev embeddings provide excellent stability on bounded intervals and better preserve sharp phase interfaces. As a result, SEDONet delivers the highest accuracy and most consistent spatio-temporal fidelity among the three operator-learning architectures.

## 4 Summary

This work introduced the Spectral-Embedded DeepONet (SEDONet), a Chebyshev-enhanced operator-learning architecture tailored to PDEs on bounded and non-periodic domains. By replacing the standard coordinate-input trunk with a fixed tensor-product Chebyshev dictionary, SEDONet injects a non-periodic spectral prior that strengthens the representation of boundary layers, steep gradients, and stiff spatio-temporal features. The branch network remains unchanged, preserving the original DeepONet framework and adding no trainable parameters. As summarized in Table 1, SEDONet achieves the lowest relative  $\ell_2$  error across all five benchmark families, elliptic, parabolic, advective-diffusive, and chaotic, consistently outperforming both a tuned DeepONet and the Fourier-Embedded DeepONet (FEDONet). On canonical non-periodic problems such as 2-D Poisson, Burgers, and advection-diffusion, the Chebyshev trunk yields noticeably sharper reconstructions and more accurate boundary resolution, while for Lorenz-96 and Allen-Cahn it provides improved temporal stability and reduced long-time drift.

Table 1: Relative  $\ell_2$  error (% , mean  $\pm$  std) for each benchmark.

Dataset	DeepONet	FEDONet	SEDONet
2-D Poisson (elliptic)	1.39 $\pm$ 0.71	1.10 $\pm$ 0.52	<b>0.97 <math>\pm</math> 0.50</b>
1-D Burgers	6.20 $\pm$ 3.08	4.47 $\pm$ 3.08	<b>3.98 <math>\pm</math> 2.64</b>
1-D Advection-Diffusion	8.00 $\pm$ 6.55	4.67 $\pm$ 4.15	<b>4.33 <math>\pm</math> 3.66</b>
Lorenz-96 (chaotic ODE)	23.63 $\pm$ 9.88	22.03 $\pm$ 8.97	<b>20.90 <math>\pm</math> 9.36</b>
Allen-Cahn (phase-field)	10.01 $\pm$ 3.46	5.70 $\pm$ 3.57	<b>5.44 <math>\pm</math> 3.05</b>

Beyond pointwise error improvements, the accompanying spectral analyses show that SEDONet more accurately reproduces the distribution of energy across scales, particularly in the high-frequency and dissipative ranges where coordinate-input trunks systematically underperform. These findings support the broader conclusion that fixed spectral embeddings, Fourier for periodic domains and Chebyshev for bounded intervals, significantly enlarge the effective hypothesis space of DeepONet. For non-periodic geometries, Chebyshev embeddings provides a more appropriate inductive bias than sinusoidal features, yielding measurable gains in accuracy, stability, and generalization. Consequently,

SEDONet provides a simple, modular, and computationally efficient enhancement to neural operator architectures, effectively bridging classical polynomial spectral methods with modern operator-learning frameworks.

## 5 Future Work

The Spectral-Embedded DeepONet (SEDONet) architecture introduces a principled way to incorporate Chebyshev polynomial structure into neural operator learning, especially for non-periodic domains. While the current formulation already demonstrates strong improvements across boundary-sensitive PDEs, several extensions offer promising directions for future investigation. A primary avenue is the development of adaptive spectral embeddings in the trunk network. In the present work, the Chebyshev dictionary is fixed; allowing the polynomial degrees, scaling factors, or spectral windowing parameters to be learned jointly with model weights could yield a more flexible representation that adjusts automatically to the local smoothness or stiffness of the underlying operator. Such adaptivity may be particularly beneficial for problems involving moving interfaces, steep gradients, or heterogeneous coefficients.

A related extension involves constructing multi-basis hybrid trunks that combine Chebyshev modes with other orthogonal families, such as Legendre polynomials, Gegenbauer polynomials, or localized wavelet packets to better capture solution behaviour exhibiting mixed regularity. For example, extending SEDONet to handle irregular geometries through domain mappings or graph-based basis functions would broaden its applicability to engineering and geophysical domains. Another promising direction is to couple the SEDONet architecture with physics-informed or uncertainty-aware training strategies. Embedding PDE residuals, conservation constraints, or Bayesian operator priors within the learning framework could improve robustness, particularly in low-data or noisy settings. In addition, integrating SEDONet with modern operator-learning paradigms such as transformer-based architectures, multi-grid neural operators, or latent operator models could further enhance generalization over long time horizons and across varying boundary conditions.

## Declaration of competing interest

The authors declare that they have no known competing financial interests or personal relationships that could have appeared to influence the work reported in this paper.

## Data availability

Data supporting the findings of this study are available from the corresponding author upon request.

## References

- [1] J. P. Boyd, Chebyshev and Fourier Spectral Methods, Courier Corporation, 2001.
- [2] D. Gottlieb, S. A. Orszag, Numerical Analysis of Spectral Methods: Theory and Applications, SIAM, 1977. doi:10.1137/1.9781611970425.
- [3] W. H. Press, S. A. Teukolsky, W. T. Vetterling, B. P. Flannery, Numerical Recipes: The Art of Scientific Computing, Cambridge University Press, 1986.
- [4] G. Cybenko, Approximation by superpositions of a sigmoidal function, Mathematics of Control, Signals and Systems 2 (4) (1989) 303–314.
- [5] K. Hornik, M. Stinchcombe, H. White, Multilayer feedforward networks are universal approximators, Neural Networks 2 (5) (1989) 359–366.
- [6] T. Poggio, F. Girosi, Networks for approximation and learning, Proceedings of the IEEE 78 (9) (1990) 1481–1497.
- [7] T. Chen, H. Chen, Universal approximation to nonlinear operators by neural networks, IEEE Transactions on Neural Networks 6 (4) (1995) 911–917.
- [8] L. Sirovich, Turbulence and the dynamics of coherent structures, Quarterly of Applied Mathematics 45 (3) (1987) 561–571.
- [9] G. Berkooz, P. Holmes, J. L. Lumley, The proper orthogonal decomposition in the analysis of turbulent flows, Annual Review of Fluid Mechanics 25 (1993) 539–575.
- [10] C. E. Rasmussen, C. K. I. Williams, Gaussian Processes for Machine Learning, MIT Press, 2005.



- [11] E. J. Kansa, Multiquadrics for scattered data approximation, *Computers & Mathematics with Applications* 19 (8) (1990) 127–145.
- [12] D. Lowe, D. Broomhead, Multivariable functional interpolation and adaptive networks, *Complex Systems* 2 (3) (1988) 321–355.
- [13] L. Lu, P. Jin, G. Pang, Z. Zhang, G. E. Karniadakis, Learning nonlinear operators via DeepONet, *Nature Machine Intelligence* 3 (2021) 218–229.
- [14] N. Kovachki, Z. Li, B. Liu, K. Azizzadenesheli, K. Bhattacharya, A. Stuart, A. Anandkumar, Neural operator: Learning maps between function spaces, *Journal of Machine Learning Research* 24 (1) (2023) 1–97.
- [15] Z. Li, N. Kovachki, K. Azizzadenesheli, B. Liu, K. Bhattacharya, A. Stuart, A. Anandkumar, Fourier neural operator for parametric PDEs (2021). [arXiv:2010.08895](https://arxiv.org/abs/2010.08895).
- [16] T. Tripura, S. Chakraborty, Wavelet neural operator, *Computer Methods in Applied Mechanics and Engineering* 404 (2023) 115783.
- [17] G. Gupta, X. Xiao, P. Bogdan, Multiwavelet-based operator learning, in: *Advances in Neural Information Processing Systems (NeurIPS)*, 2021.
- [18] J. Kossaifi, N. Kovachki, K. Azizzadenesheli, A. Anandkumar, Multi-grid tensorized fourier neural operator, *arXiv preprint arXiv:2310.00120* (2023).
- [19] Z.-H. Guo, H.-B. Li, MgFNO: Multi-grid architecture fourier neural operator (2024). [arXiv:2407.08615](https://arxiv.org/abs/2407.08615).
- [20] Z. Li, N. Kovachki, K. Azizzadenesheli, B. Liu, K. Bhattacharya, A. Stuart, A. Anandkumar, Neural operator: Graph kernel network (2020). [arXiv:2003.03485](https://arxiv.org/abs/2003.03485).
- [21] Z. Li, N. Kovachki, K. Azizzadenesheli, B. Liu, K. Bhattacharya, A. Stuart, A. Anandkumar, Multipole graph neural operator (2020). [arXiv:2006.09535](https://arxiv.org/abs/2006.09535).
- [22] Z. Li, D. Z. Huang, B. Liu, A. Anandkumar, Fourier neural operator with learned deformations, *Journal of Machine Learning Research* 24 (388) (2023) 1–26.
- [23] Z. Li, N. Kovachki, C. Choy, B. Li, J. Kossaifi, S. Otta, M. A. Nabian, M. Stadler, C. Hundt, K. Azizzadenesheli, et al., Geometry-informed neural operator, *Advances in Neural Information Processing Systems (NeurIPS)* (2023).
- [24] J. Huang, K. Zhang, Y. Wu, Z. Cheng, Operator learning with domain decomposition for geometry generalization (2025). [arXiv:2504.00510](https://arxiv.org/abs/2504.00510).
- [25] S. E. Ahmed, P. Stinis, A multifidelity deep operator network approach to closure for multiscale systems, *Computer Methods in Applied Mechanics and Engineering* 414 (2023) 116161. doi:10.1016/j.cma.2023.116161.
- [26] A. A. Howard, M. Perego, G. E. Karniadakis, P. Stinis, Multifidelity deep operator networks for data-driven and physics-informed problems, *Journal of Computational Physics* 493 (2023) 112462. doi:10.1016/j.jcp.2023.112462.
- [27] P. Battle, M. Darcy, B. Hosseini, H. Owhadi, Kernel methods are competitive for operator learning, *Journal of Computational Physics* 496 (2024) 112549. doi:10.1016/j.jcp.2023.112549.
- [28] S. Kumar, R. Nayek, S. Chakraborty, Neural operator induced gaussian process framework for probabilistic solution of parametric partial differential equations, *Computer Methods in Applied Mechanics and Engineering* 431 (2024) 117265. doi:10.1016/j.cma.2024.117265.
- [29] S. Garg, S. Chakraborty, Neuroscience inspired neural operator for partial differential equations, *Journal of Computational Physics* 515 (2024) 113266. doi:10.1016/j.jcp.2024.113266.
- [30] T. O’Leary-Roseberry, Y. Chen, U. Villa, O. Ghattas, Derivative-informed neural operator: An interpretable neural operator architecture for learning parametric differential operators, *Journal of Computational Physics* 496 (2024) 112555. doi:10.1016/j.jcp.2023.112555.
- [31] X. Liu, B. Xu, S. Cao, L. Zhang, Mitigating spectral bias for the multiscale operator learning, *Journal of Computational Physics* 506 (2024) 112944. doi:10.1016/j.jcp.2024.112944.
- [32] S. Wu, A. Zhu, Y. Tang, B. Lu, Solving parametric elliptic interface problems via interfaced operator network (IONet), *Journal of Computational Physics* 514 (2024) 113217. doi:10.1016/j.jcp.2024.113217.
- [33] X. Bi, X. Chen, C. Zhao, Q. Li, J. Zhang, XI-DeepONet: An operator learning method for elliptic interface problems, *Journal of Computational Physics* 538 (2025) 114164. doi:10.1016/j.jcp.2024.114164.
- [34] X. Li, T. Tripura, S. Chakraborty, Local neural operator for solving transient partial differential equations on varied domains, *Computer Methods in Applied Mechanics and Engineering* 427 (2024) 117062. doi:10.1016/j.cma.2024.117062.

- [35] J. Huang, Y. Qiu, Resolution invariant deep operator network for PDEs with complex geometries, *Journal of Computational Physics* 522 (2025) 113601. doi:10.1016/j.jcp.2024.113601.
- [36] Y. Meng, J. Huang, Y. Qiu, Koopman operator learning using invertible neural networks, *Journal of Computational Physics* 501 (2024) 112795. doi:10.1016/j.jcp.2024.112795.
- [37] S. Jafarzadeh, S. Silling, N. Liu, Z. Zhang, Y. Yu, Peridynamic neural operators: A data-driven nonlocal constitutive model for complex material responses, *Computer Methods in Applied Mechanics and Engineering* 425 (2024) 116914. doi:10.1016/j.cma.2024.116914.
- [38] W. Chen, P. Stinis, Feature-adjacent multi-fidelity physics-informed machine learning for partial differential equations, *Journal of Computational Physics* 498 (2024) 112683. doi:10.1016/j.jcp.2023.112683.
- [39] S. Jafarzadeh, S. Silling, N. Liu, Z. Zhang, Y. Yu, Peridynamic neural operators: A data-driven nonlocal constitutive model for complex material responses, *Computer Methods in Applied Mechanics and Engineering* 425 (2024) 116914. doi:10.1016/j.cma.2024.116914.
- [40] X. Dong, C. Chen, J.-L. Wu, Data-driven stochastic closure modeling via conditional diffusion model and neural operator, *Journal of Computational Physics* 534 (2025) 114005. doi:10.1016/j.jcp.2025.114005.
- [41] B. Bahmani, S. Goswami, I. G. Kevrekidis, M. D. Shields, A resolution independent neural operator, *Computer Methods in Applied Mechanics and Engineering* 444 (2025) 118113.
- [42] H. Li, X. Ye, P. Jiang, G. Qin, T. Wang, Local neural operator for solving transient partial differential equations on varied domains, *Computer Methods in Applied Mechanics and Engineering* 427 (2024) 117062. doi:10.1016/j.cma.2024.117062.
- [43] W. Zhong, H. Meidani, Physics-informed geometry-aware neural operator, *Computer Methods in Applied Mechanics and Engineering* 415 (2023) 116278. doi:10.1016/j.cma.2023.116278.
- [44] X. Xu, J. Guilleminot, V. Tarokh, Neural operators from the cole-hopf transformation: Leveraging relations between pdes for efficient operator learning, *Computer Methods in Applied Mechanics and Engineering* (2025).
- [45] S. Goswami, Z. Li, K. Azizzadenesheli, M. Liu-Schiaffini, K. Bhattacharya, H. Hassani, A. M. Stuart, A. Anandkumar, Physics-informed deep operator networks (2022). arXiv:2207.05748.
- [46] Z. Li, N. Kovachki, K. Azizzadenesheli, K. Bhattacharya, A. M. Stuart, A. Anandkumar, Physics-informed neural operator (2023). arXiv:2309.15502.
- [47] M. S. Eshaghi, P. Akhtari, G. E. Karniadakis, Variational physics-informed neural operator (2024). arXiv:2403.08377.
- [48] K. Chen, M. Zhao, W. Li, G. Lin, Pseudo physics-informed neural operators (2025). arXiv:2501.01234.
- [49] T. Wang, C. Wang, Latent neural operators (2024). arXiv:2404.00967.
- [50] T. Wang, C. Wang, Latent neural operator pretraining (2024). arXiv:2408.05677.
- [51] Z. Ahmad, N. Kovachki, Z. Li, A. M. Stuart, A. Anandkumar, Diffeomorphic latent neural operators (2024). arXiv:2406.01411.
- [52] D. Long, Y. Rao, J. Lu, J. Zhou, Invertible fourier neural operators (2025). arXiv:2502.04521.
- [53] N. Cho, J. Ryu, H. J. Hwang, Sobolev training for operator learning, *Journal of Computational Physics* 543 (2025) 114408. doi:10.1016/j.jcp.2025.114408.
- [54] H. Huang, R. Lai, Unsupervised solution operator learning for mean-field games, *Journal of Computational Physics* 537 (2025) 114057. doi:10.1016/j.jcp.2025.114057.
- [55] L. Yang, S. Osher, Pde generalization of in-context operator networks: A study on 1d scalar nonlinear conservation laws, *Journal of Computational Physics* 519 (2024) 113379. doi:10.1016/j.jcp.2024.113379.
- [56] N. Rahaman, A. Baratin, D. Arpit, F. Draxler, M. Lin, F. A. Hamprecht, Y. Bengio, A. Courville, On the spectral bias of neural networks (2019). arXiv:1806.08734.
- [57] M. Tancik, P. P. Srinivasan, B. Mildenhall, S. Fridovich-Keil, N. Raghavan, U. Singhal, R. Ramamoorthi, J. T. Barron, R. Ng, Fourier features for learning high frequency functions (2020). arXiv:2006.10739.
- [58] M. Kast, J. S. Hesthaven, Positional embeddings for solving PDEs, *Journal of Computational Physics* 505 (2024) 112924.
- [59] A. Sojitra, M. Dhingra, O. San, Fedonet: Fourier-embedded deepnet for spectrally accurate operator learning, arXiv preprint arXiv:2509.12344 (2025).

- [60] Z. Liu, H. Wang, H. Zhang, K. Bao, X. Qian, S. Song, Render unto numerics: Orthogonal polynomial neural operator for pdes with nonperiodic boundary conditions, *SIAM Journal on Scientific Computing* 46 (4) (2024) C323–C348.
- [61] S. Mall, S. Chakraverty, Single layer Chebyshev neural network, *Neural Computing and Applications* 28 (2017) 915–929.
- [62] S. M. Sivalingam, P. Kumar, V. Govindaraj, Chebyshev neural network for fractional PDEs, *Computers & Mathematics with Applications* (2024).
- [63] P. Yin, S. Ling, W. Ying, Chebyshev spectral neural networks for solving partial differential equations, *arXiv preprint arXiv:2407.03347* (2024).
- [64] Y. Huang, H. Liu, Y. Zhao, M. Fei, Chebyshev spectral approximation-based physics-informed neural network for solving higher-order nonlinear differential equations, *Engineering with Computers* 41 (2) (2025) 1191–1210.
- [65] S. Chen, S. Xiong, Y. Liu, Chebyshev-sobolev physics-informed neural networks for general pde solutions, *International Journal of Applied and Computational Mathematics* 11 (5) (2025) 169.
- [66] H. Zhang, Y. Wang, AC-PKAN: Attention-enhanced and chebyshev polynomial kolmogorov-arnold networks for physics-informed learning, in: *Proceedings of the International Conference on Learning Representations (ICLR)*, 2024, openReview preprint.
- [67] Z. Xu, Y. Chen, D. Xiu, Chebyshev feature neural network for accurate function approximation, *arXiv preprint arXiv:2409.19135* (2024).
- [68] V. S. Fanaskov, I. V. Oseledets, Spectral neural operators, in: *Doklady Mathematics*, Vol. 108, Springer, 2023, pp. S226–S232.

## A Spectral Properties of Chebyshev Embeddings

In this appendix we summarize a few classical spectral properties of Chebyshev polynomials that underpin the design of the SEDONet trunk. The goal is not to provide an exhaustive review, but to highlight the aspects that directly influence conditioning, approximation quality, and the behavior of the fixed embedding  $\phi_{\text{Cheb}}(x, t)$  used in Section 2.

### A.1 Orthogonality and Conditioning

The Chebyshev polynomials of the first kind  $\{T_n(\xi)\}_{n \geq 0}$  form an orthogonal basis on  $[-1, 1]$  with respect to the weight  $w(\xi) = (1 - \xi^2)^{-1/2}$ :

$$\int_{-1}^1 \frac{T_m(\xi) T_n(\xi)}{\sqrt{1 - \xi^2}} d\xi = \begin{cases} 0, & m \neq n, \\ \pi, & m = n = 0, \\ \frac{\pi}{2}, & m = n \geq 1. \end{cases} \quad (28)$$

This relation implies that low- and high-order modes are well-separated when integrated against the Chebyshev weight. In SEDONet, the trunk embedding  $\phi_{\text{Cheb}}(x, t)$  is constructed from tensor products of these polynomials evaluated at mapped coordinates  $(\xi_x, \xi_t)$ . When  $(x, t)$  are sampled close to Gauss-Lobatto collocation points, the resulting feature matrix

$$\Phi = \begin{bmatrix} \phi_{\text{Cheb}}(x^1, t^1)^\top \\ \vdots \\ \phi_{\text{Cheb}}(x^Q, t^Q)^\top \end{bmatrix} \in \mathbb{R}^{Q \times d_{\text{trunk}}}$$

has nearly orthogonal columns. Equivalently, also the empirical Gram matrix that is shown as follows below

$$G = \frac{1}{Q} \sum_{q=1}^Q \phi_{\text{Cheb}}(x^q, t^q) \phi_{\text{Cheb}}(x^q, t^q)^\top$$

is close to diagonal and well-conditioned. This “near-orthogonality” plays a role similar to the whitening effect of random Fourier features, but it is specifically adapted to bounded, non-periodic domains and remains stable near boundaries where standard polynomial bases often become ill conditioned.

## A.2 Spectral Convergence on Bounded Domains

Let  $f : [-1, 1] \rightarrow \mathbb{R}$  be a sufficiently smooth function. Then its Chebyshev expansion representation as follows

$$f(\xi) \approx \sum_{n=0}^{K-1} a_n T_n(\xi)$$

converges at a spectral (geometric) rate as  $K \rightarrow \infty$ . For analytic  $f$ , the Chebyshev coefficients  $a_n$  decay faster than any algebraic rate, and the approximation error decreases accordingly. For functions of two variables, tensor-product bases  $\{T_i(\xi_x)T_j(\xi_t)\}$  provide the same rapid convergence on  $[-1, 1]^2$  after the affine mapping  $(x, t) \mapsto (\xi_x, \xi_t)$ .

In SEDONet, the fixed Chebyshev embedding  $\phi_{\text{Cheb}}(x, t)$  therefore supplies a rich dictionary capable of spectrally approximating smooth PDE solutions defined on bounded domains. The trunk network  $\Psi_\theta$  learns nonlinear mixtures of these polynomial modes, while the branch network  $B_\theta$  maps input functions to corresponding coefficients. Together they realize a data-driven Chebyshev-type expansion adapted to the target operator, as formalized in the spectral interpretation (15).

## B Theoretical Justification for the Chebyshev Embedding Superset Property

We now discuss, at a functional level, why the hypothesis space induced by Chebyshev embeddings is richer than the one obtained from direct coordinate-input networks on bounded domains:

$$\mathcal{H}_{\text{vanilla}} \subsetneq \mathcal{H}_{\text{Cheb}}.$$

The argument is intentionally high level and is meant to provide intuition rather than a fully measure-theoretic proof. For simplicity, we work in one spatial dimension  $x \in [0, 1]$ . The extension to higher dimensions via the tensor-product construction in (8) is straightforward.

### Function Classes

A vanilla coordinate-input neural network for parameters  $(a_j, w_j, b_j)$  and nonlinear activation  $\sigma$  represents functions of the form

$$f(x) = \sum_{j=1}^N a_j \sigma(w_j x + b_j), \quad (29)$$

We denote by  $\mathcal{H}_{\text{vanilla}}$  the set of all such functions for a given architecture (including the fixed depth and also the width).

A Chebyshev-embedded network first maps  $x \in [0, 1]$  to  $\xi = 2x - 1 \in [-1, 1]$  and uses the truncated Chebyshev feature vector

$$\phi_{\text{Cheb}}(x) = [T_0(\xi), T_1(\xi), \dots, T_{K-1}(\xi)]^\top, \quad (30)$$

so that the network outputs

$$g(x) = \sum_{j=1}^M \alpha_j \sigma(v_j^\top \phi_{\text{Cheb}}(x) + \beta_j), \quad (31)$$

for parameters  $(\alpha_j, v_j, \beta_j)$ . We denote the corresponding function class by  $\mathcal{H}_{\text{Cheb}}$ .

### Part I: Inclusion

$$\mathcal{H}_{\text{vanilla}} \subseteq \mathcal{H}_{\text{Cheb}}$$

Universal approximation guarantees that any continuous function  $f$  on  $[0, 1]$  can be approximated arbitrarily well by a polynomial  $P(x)$ : for every  $\varepsilon > 0$  there exists a polynomial  $P$  such that

$$\sup_{x \in [0, 1]} |f(x) - P(x)| < \varepsilon/2.$$

So, the every polynomial  $P(\xi)$  on the domain  $[-1, 1]$  can in turn be written exactly as a Chebyshev series as follows

$$P(\xi) = \sum_{n=0}^{K-1} c_n T_n(\xi),$$

for some coefficients  $c_n$ . Consequently,  $P(x)$  can be expressed as a linear functional of the Chebyshev feature map (30). A Chebyshev-embedded network can therefore reproduce  $P(x)$  (up to floating-point precision) using a single linear neuron applied to  $\phi_{\text{Cheb}}(x)$ . Thus for any  $\varepsilon > 0$  there exists  $\tilde{f} \in \mathcal{H}_{\text{Cheb}}$  with for the following property that is

$$\sup_{x \in [0,1]} |f(x) - \tilde{f}(x)| < \varepsilon,$$

showing that the following that is  $(\mathcal{H}_{\text{vanilla}} \subseteq \mathcal{H}_{\text{Cheb}})$ , in terms of uniform approximation on the interval  $[0, 1]$ .

## Part II: Strictness

$$\mathcal{H}_{\text{vanilla}} \subsetneq \mathcal{H}_{\text{Cheb}}$$

To see that the inclusion is strict for a fixed neural architecture, consider the high-degree Chebyshev mode of the form

$$f_K(x) = T_K(\xi), \quad \xi = 2x - 1. \quad (32)$$

By construction,  $f_K(x) = [\phi_{\text{Cheb}}(x)]_K$ , so  $f_K$  is realized in  $\mathcal{H}_{\text{Cheb}}$  exactly with a single linear neuron on top of the embedding.

From the perspective of  $x$ , however,  $f_K(x)$  is a degree- $K$  polynomial. To represent such a function using the coordinate-input network (29) with fixed depth and width, the network must emulate increasingly high-order polynomial behavior through compositions of affine maps and nonlinearities. As  $K$  grows, this requires either a larger number of neurons or deeper composition; otherwise, approximation error cannot be made arbitrarily small.

Informally, this means that for any fixed vanilla architecture there are degrees  $K$  for which  $f_K$  belongs to  $\mathcal{H}_{\text{Cheb}}$  but cannot be approximated within a prescribed tolerance without increasing the capacity of the coordinate-input network. Hence, at fixed network size,

$$\mathcal{H}_{\text{vanilla}} \subsetneq \mathcal{H}_{\text{Cheb}}.$$

This discussion formalizes the expressivity advantage exploited by SEDONet: Chebyshev embeddings provide direct access to high-order, non-periodic polynomial modes that are difficult for coordinate-input MLPs to learn efficiently. As a consequence, SEDONet is particularly effective for PDEs on bounded domains with sharp gradients or boundary layers, where polynomial spectral representations naturally arise.